International Journal of Nanomedicine

Dovepress
open access to scientific and medical research

Open Access Full Text Article

ORIGINAL RESEARCH

Anti-Inflammatory Effects of Magnetically Targeted Mesenchymal Stem Cells on Laser-Induced Skin Injuries in Rats

This article was published in the following Dove Press journal:
International Journal of Nanomedicine

Xiuying Li[1,*]
Zhenhong Wei[1,*]
Wei Zhang[2]
Huiying Lv[1]
Jing Li[1]
Liya Wu[1]
Hao Zhang[3]
Bai Yang[3]
Mingji Zhu[4]
Jinlan Jiang[1]

[1]Scientific Research Center, China-Japan Union Hospital of Jilin University, Changchun, Jilin, People's Republic of China; [2]Department of Radiotherapy, The Second Hospital of Jilin University, Changchun, Jilin, People's Republic of China; [3]State Key Laboratory of Supramolecular Structure and Materials, College of Chemistry, Jilin University, Changchun, Jilin, People's Republic of China; [4]Dermatological Department, China-Japan Union Hospital of Jilin University, Changchun, Jilin, People's Republic of China

*These authors contributed equally to this work

Correspondence: Jinlan Jiang
Scientific Research Center, China-Japan Union Hospital of Jilin University, No. 126 Xiantai Street, Changchun 130033, Jilin, People's Republic of China
Email jiangjinlan@jlu.edu.cn

Mingji Zhu
Dermatological DepartmentNo. 126 Xiantai Street, Changchun 130033, Jilin, People's Republic of China
Tel/Fax +86 04 318 499 5423
Email zmj@jlu.edu.cn

Introduction: Mesenchymal stem cells (MSCs) are a promising resource for tissue regeneration and repair. However, their clinical application is hindered by technical limitations related to MSC enrichment at the target sites.

Methods: MSCs were labeled with magnetic Fe_3O_4 nanoparticles (NPs). We analyzed the effects of NP on cell proliferation, stem cell characteristics, and cytokine secretion. Furthermore, we induced NP-labeled MSC migration with an external magnetic field toward laser-induced skin wounds in rats and evaluated the associated anti-inflammatory effects.

Results: Fe_3O_4 NP application did not adversely affect MSC characteristics. Moreover, Fe_3O_4 NP-labeled MSCs presented increased anti-inflammatory cytokine and chemokine production compared with unlabeled MSCs. Furthermore, MSCs accumulated at the injury site and magnetic targeting promoted NP-labeled MSC migration toward burn injury sites in vivo. On day 7 following MSC injection, reduced inflammation and promoted angiogenesis were observed in the magnetically targeted MSC group. In addition, anti-inflammatory factors were upregulated, whereas pro-inflammatory factors were downregulated within the magnetically targeted MSC group compared with those in the PBS group.

Conclusion: This study demonstrates that magnetically targeted MSCs contribute to cell migration to the site of skin injury, improve anti-inflammatory effects and enhance angiogenesis compared with MSC injection alone. Therefore, magnetically targeted MSC therapy may be an effective treatment approach for epithelial tissue injuries.

Keywords: mesenchymal stem cells, skin injury, magnetic targeting, Fe_3O_4 nanoparticle, anti-inflammatory effect

Introduction

With the development of regenerative technologies, stem cell therapy has emerged as a promising and attractive strategy to enhance tissue regeneration, cutaneous homeostasis, and wound healing.[1–4] Bone marrow-derived mesenchymal stem cells (BM-MSCs), also known as stromal progenitor cells, possess the ability to self-renew, expand rapidly, and differentiate into various tissue types via asymmetric replication.[5–7] Mesenchymal stem cells (MSCs) express low levels of major histocompatibility complex molecules, and this allows their allogeneic and xenogeneic applications.[8] MSCs are involved in the inflammatory, proliferating and remodeling stages of tissue regeneration.[9–11] Additionally, tissue injury repair is primarily advanced by MSCs that migrate to the site of damage and undergo differentiation, thereby promoting structural and functional repair.[12] The homing capacity of MSCs allows them to migrate to sites of

© 2020 Li et al. This work is published and licensed by Dove Medical Press Limited. The full terms of this license are available at https://www.dovepress.com/terms.php and incorporate the Creative Commons Attribution – Non Commercial (unported, v3.0) License (http://creativecommons.org/licenses/by-nc/3.0/). By accessing the work you hereby accept the Terms. Non-commercial uses of the work are permitted without any further permission from Dove Medical Press Limited, provided the work is properly attributed. For permission for commercial use of this work, please see paragraphs 4.2 and 5 of our Terms (https://www.dovepress.com/terms.php).

injury and inflammation.[13] Several studies have demonstrated that after intravenous delivery, BM-MSCs migrate to the site of bone or cartilage damage, myocardial infarction, and ischemic cerebral injury.[14–16] Although MSCs were initially shown to promote tissue repair by trans-differentiation of specific cell types required to repair damaged tissue, current data suggest paracrine signaling as the primary mediator of the reparative effects of MSCs.[17] Practically, attracting more cells to a damaged tissue would enhance the recovery of the injured tissue because of the increase in paracrine factors. Thus, increasing the migratory capacity of MSCs would improve healing.

Severe acute skin injuries such as those caused by burns and chronic wounds are a global health issue.[18] Wound healing progresses via various overlapping phases of cell migration, inflammation, angiogenesis, proliferation, and remodeling.[19,20] MSCs enhance angiogenesis in the wound healing process.[21] In fact, a study involving MSCs implanted into cutaneous wounds suggested that MSCs increase the levels of vascular endothelial growth factor (VEGF), one of the most potent pro-angiogenic factors, the density of microvessels, and cutaneous wound microcirculation.[22] However, the regression of inflammation is the key to successful wound healing, because chronic inflammation can lead to poor healing.[23,24] The administration of MSCs attenuates inflammation, reduces pro-inflammatory network activity, and amplifies anti-inflammatory signals.[25] Thus, the ability of MSCs to regulate inflammatory responses supports their beneficial effects on the healing response.

The strong anti-inflammatory potential of MSCs in skin wound healing has encouraged efforts to identify and develop suitable MSC delivery approaches. Recent studies have also assessed new approaches to maximize MSC migratory capacity.[26–29] Specifically, strategies to increase MSC migration to areas of skin trauma have been investigated.[28,29] C-X-C chemokine receptor type 4 (CXCR4) overexpression enhanced MSC migration to damaged tissue sites in vivo.[30] Other studies have attempted to improve homing efficiency by binding specific antibodies or proteins to the cell surface.[26,27] Previous studies on *Mallotus philippinensis* bark extract have similarly demonstrated enhanced MSC migration to wound sites via blood circulation.[31] However, these experimental methods and processes are very complicated. Therefore, finding a simple and convenient way to increase the homing ability of MSCs is the direction of ongoing research efforts.

Recently, a magnetically targeting drug delivery system has been developed to improve drug targeting, enhance drug efficacy, and reduce toxic adverse effects.[32,33] Iron oxide nanoparticles (NPs) are a transmission medium-based magnetic targeting drug delivery system.[34,35] Magnetic MSCs were obtained by co-cultivating MSCs with diluted magnetic NPs in cell culture medium. The MSCs internalize the NPs by passive diffusion or endocytosis, generally over a few hours.[36] Iron-containing NPs show an acceptable level of biocompatibility, partially due to the body's innate ability to metabolize naturally occurring iron in the form of ferritin. Because iron-containing NPs are superparamagnetic, the risks of particle aggregation and vessel occlusion are minimized.[37] Another reason for good biocompatibility is that NPs may have an activity similar to that of natural catalases, and it depends on the acidity of the surrounding cellular environment.[38] Shen et al introduced another method to deliver magnetic stem cells via intra-carotid delivery, thereby improving attraction to injured areas after traumatic brain injury.[39] Although these results are promising, most of these studies used a constant electromagnetic or an internal magnetic field.

There are a few studies on the application of permanent transient non-invasive external magnetic fields (EMF) to magnetically targeted MSC therapy. Iron (II,III) oxide (Fe_3O_4) in iron oxide NPs can be employed to induce directional migration of magnetized MSCs using an EMF.[40] Therefore, in this study, we sought to (i) determine if MSCs labeled with Fe_3O_4 NPs retain their biological characteristics, (ii) detect the secretion of anti-inflammatory cytokines after treatment with MSCs labeled with Fe_3O_4 NPs, and (iii) assess the migration of magnetically targeted MSCs and their therapeutic effect on burned skin in vivo. Our results indicate that Fe_3O_4 NPs have no adverse effects on MSCs and increase anti-inflammatory cytokine production in MSCs in vitro. In addition, we revealed that magnetically targeted MSCs had better effects on migration, angiogenesis and anti-inflammatory cytokine secretion than MSCs alone, suggesting that magnetically targeted MSCs had stronger anti-inflammatory effects on burned skin repair in vivo (Figure 1).

Materials and Methods

Iron acetylacetonate (Fe $(acac)_3$, 99.9+%), 1,2-hexadecanediol (90%), benzyl ether (99%), oleyamine (OLA, 70%), oleic acid (OA, 90%), and sodium dodecyl sulfate (SDS, 99%) were purchased from Sigma-Aldrich. Toluene was analytical grade and used as received. Absolute ethanol and deionized water were used in all experiments.

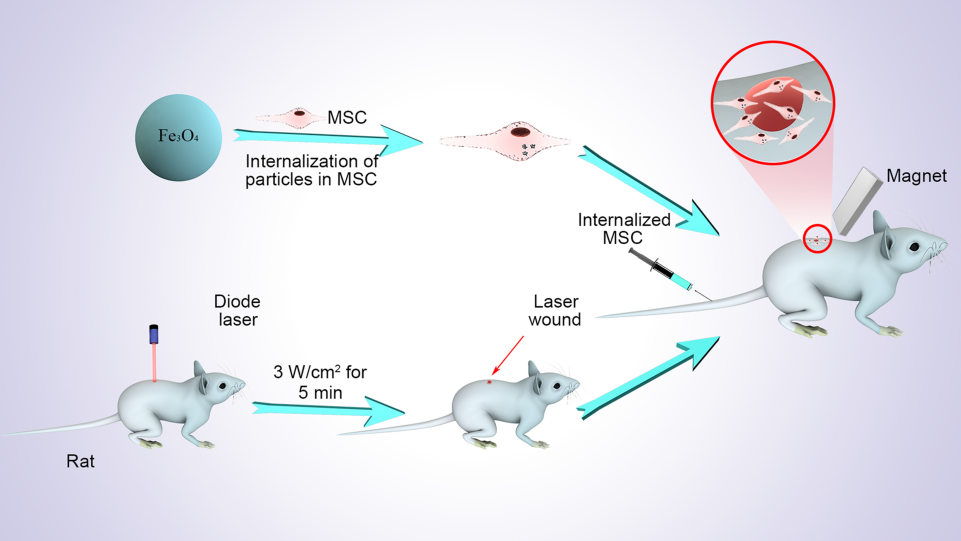

Figure 1 Schematic diagram of the entire experiment.

Ethical Approval

The rats were treated in strict accordance with the Guidelines for the Care and Use of Experimental Animals of Jilin University. The protocol was approved by the Animal Experimental Ethics Committee of Jilin University (Experiment no. SY201807024). All animal experiments were conducted in accordance with internationally recognized guidelines for animal care (EEC Directive of 1986; 86/609/EEC).

Synthesis of Fe_3O_4 NPs

We mixed 5 mmol 1, 2-hexadecanediol, 2 mmol Fe $(acac)_3$, 6 mmol OA, and 6 mmol OLA with 20 mL of benzyl ether. Under a nitrogen atmosphere, the mixture was heated to 200 ºC at a rate of 20 ºC min^{-1} for 30 min, and then refluxed for another 30 min at 265 ºC. The solution was then cooled to room temperature. The OA-stabilized Fe_3O_4 NPs were extracted and washed three times with ethanol before being dispersed in toluene. Under mechanical stirring and a nitrogen atmosphere at room temperature, 4.0 mL of 7.0 mg/mL OA-stabilized Fe_3O_4 NPs were injected into aqueous SDS solution (2.8 mg/mL, 12.5 mL). After ultrasonic treatment, the emulsion was heated at 60 ºC to evaporate toluene. The SDS-capped Fe_3O_4 NPs were collected and stored at 4°C in a refrigerator until use. Dynamic light scattering was measured using Zetasizer Nano ZS (Malvern Instruments, Worcestershire, U.K.).

BM-MSC Isolation

BM-MSCs were harvested from the bone marrow of 4-week-old male Wistar rats, as previously described.[41] Briefly, the rats were euthanized, and then the tibias and femurs were collected and cleaned to remove connective tissues. After removing the epiphysis, the marrow was flushed out and cultured in DMEM/F12 supplemented with 10% fetal bovine serum (FBS, Invitrogen Australia Pty Ltd., Mount Waverley, Victoria, Australia) and 1% penicillin/streptomycin. The marrow was then incubated at 37°C in a humidified 5% CO_2 environment. The medium was changed twice weekly until the cells reached approximately 80% confluence. The third or fourth passages' MSCs were used in all experiments.

MSC Characteristics

The third passage cells were used for MSC differentiation and surface marker detection. Adipogenesis or osteogenesis was validated via independent experiments using complete STEMPRO® adipogenesis or osteogenesis differentiating medium (Invitrogen Australia Pty Ltd.), according to the manufacturer's protocol. Following fixation, the lipids in cells were detected by Oil Red O staining (Sigma-Aldrich, St. Louis, MO, USA). Cells in osteogenic cultures were stained with Alizarin red using the Alizarin staining kit (Genmed, Shanghai, China). Flow cytometry analysis was performed for MSC identification. The antibodies used were as follows: anti-cluster of differentiation (CD) 73 (nbp2-25235SS; Novus, Colorado, USA), CD105 (ab11414; Abcam, Cambridge, UK), CD34 (ab81289; Abcam), fluorescein isothiocyanate (FITC) CD45 (561867, BD Biosciences; CA, USA), CD44 (550974; BD Biosciences) and FITC-CD90 (561973; BD

Biosciences). The cells were then incubated with goat anti-rabbit IgG-FITC or anti-mouse IgG/PE secondary antibodies (abs20023/abs20007; Absin, Shanghai, China). Data were analyzed by flow cytometry (FACSAria II; Becton Dickinson, New Jersey, USA) with FACSDiva software (Becton Dickinson).

In vitro Cell Labeling and Toxicity Assays

Adherent MSCs (80–90% confluence) were washed with phosphate-buffered saline (PBS) and incubated with Fe_3O_4 NPs (0, 25, 50, 100, 150, and 200 μg/mL) in FBS-free culture medium for 2 h (n = 4). The cells and NPs were then co-cultured in a fresh medium containing 10% FBS for 14 h. The MSCs were washed with PBS and stained using the Prussian blue iron staining kit (Beijing Solarbio Science and Technology, Co. Ltd., Beijing, China), according to the manufacturer's protocol.

In vitro toxicity experiments were performed at 24 h after Fe_3O_4 NP (0, 25, 50, 100, 150, and 200 μg/mL) labeling. Cytotoxicity of Fe_3O_4 NPs was evaluated using the cell counting kit (CCK)-8 assay (KeyGEN BioTECH, Nanjing, China). Fe_3O_4 NPs that displayed minimal cytotoxicity were used in the subsequent experiments.

Quantification of Intracellular Iron

To quantify the cellular uptake of Fe_3O_4 NPs, the iron content in NP-labeled MSCs was detected by inductively coupled plasma-optical emission spectrometry (ICP-OES) using the Perkin-Elmer Optima 3300DV system (Perkin-Elmer, Shelton, CT, USA) after digestion in 70% nitric acid and 30% hydrogen peroxide.

Transmission Electron Microscopy (TEM) Analysis

The morphological structure of Fe_3O_4 NPs (100 μg/mL) was examined using the Hitachi H-800 Electron Microscope (Hitachi, Tokyo, Japan) equipped with a charge-coupled device camera operating at an acceleration voltage of 200 kV. For TEM, the cells were fixed in phosphate-buffered Karnofsky's fixative solution, stained with 2% osmium tetroxide over night at 4°C, dehydrated, embedded in epoxy resin, and cut into 70-nm sections. The sections were collected on copper grids containing Formvar support film. The samples were analyzed using the Tecnai Spirit system (120 kV; FEI, Hillsboro, OR, USA).

Proliferation Assay

The third passage cells were used in the proliferation assay. The proliferation of NP-labeled and unlabeled MSCs was compared using the CCK-8 assay. MSCs labeled with or without Fe_3O_4 NPs (50 μg/mL) were seeded in 96-well plates (5000 cells/cm^2). After 1, 3, 5, and 7 days, the cells were evaluated by measuring the optical density (OD) at 450 nm using a microplate reader (Bio-Rad Laboratories Inc., Hercules, CA, USA).

Colony Formation Assay

The third passage cells were used in the colony formation assay. To test clonogenicity, MSCs labeled with and without NPs were seeded in six well plates (200 cells/well) in the growth medium, which was changed every 3 days. Colonies were allowed to form. Next, the colonies were counted and analyzed within 15 days after seeding. MSCs were washed to remove non-adherent colonies. The colonies were then fixed in 4% paraformaldehyde, stained with Giemsa stain (Sigma-Aldrich), and manually counted.

Luminex Analysis

The cytokines' concentrations in collected culture supernatants or serum samples were determined using the Luminex assay with the rat multiplex-cytokine kits (LXSARM-17; R&D Systems Inc., MN, USA). All samples were assayed in duplicate. Briefly, culture supernatants or serum samples were thawed to 4°C and centrifuged at 4°C for 3 min at 1000 *g* to settle any residue. Antibody-coated beads were added to 50 μL of standards and samples in microtiter filter plates. The samples were incubated for 2 h at 23−25°C with continuous shaking at 800 rpm. The plate was then washed and incubated with detection antibodies for 1 h at 23−25°C followed by another 30 min of incubation with streptavidin-labeled PE. The plate was washed twice, and then sheath fluid was added to each well. Finally, the plate was read using a Luminex 200 plate reader. Standard curves were automatically constructed using the five-parameter logistic method. Cytokine concentrations in experimental samples were calculated using the generated standard curves.

Quantitative Reverse Transcription-Polymerase Chain Reaction (qRT-PCR)

The total RNA from tissues or cells was extracted using Trizol reagent (Life Technologies, Carlsbad, CA, USA). RNA integrity was electrophoretically verified by ethidium bromide

staining and using the OD260/OD280 nm absorption ratio (OD > 1.9). The total RNA (500 ng) was reverse transcribed into cDNA using Reverse Transcriptase II (TaKaRa, Beijing, China). A no amplification control, without added reverse transcriptase, was included. The reaction mixtures were incubated at 42°C for 30 min, then at 95°C for 5 min and at 5°C for 5 min. Twenty five nanograms of cDNA was subjected to qRT-PCR using the SYBR® Green PCR Master Mix (Applied Biosystems, Warrington, UK) with the StepOnePlus RT-PCR system (AB Applied Biosystems). The thermocycler parameters were as follows: 95°C for 5 min, followed by 40 cycles at 95°C for 15 s, 55°C for 15 s, and 72°C for 30 s. All primer sequences were designed and generated by Sangon Biotechnology (Shanghai, China). Detailed information of primers is presented in Table 1. Each sample was tested in triplicate. Relative expression was calculated using the comparative $2^{-\Delta\Delta CT}$ method.

Animal Studies

In this study, pathogen-free, 6-week-old male Wistar rats were used to avoid potential variability from the female estrous cycle. All animals were purchased from the Institute of Laboratory Animal Sciences (Beijing, China). The rats were housed under specific pathogen-free conditions to acclimate to the experimental conditions for 1 week. The back fur of the rats was removed using depilatory cream and a razor, after which the burn model was established. The rats were anesthetized with 5% chloral hydrate and ethyl ether. Then, a burn encompassing the full skin thickness was induced on the back (3 W/cm^2 for 5 min) using an 808-nm diode laser (LEO Photonics Co. Ltd., China). The rats were randomly divided into the following five groups: Group 1: blank control group intravenously injected with PBS (n = 8); Group 2: intravenous injection with MSCs dyed with 5 μM 1,1-dioctadecyl-3,3,3,3-tetramethylindodicarbocyanine (DiD) tracer (Sigma-Aldrich, St. Louis, MO, USA) (n = 8); Group 3: intravenous injection with NP-labeled MSCs dyed with DiD (n = 8); Group 4: intravenous injection with NP-labeled MSCs dyed with DiD, with a 1.2-T ultrastrong magnet placed under the injury site for 30 min (n = 8) (the rats were anesthetized for the entire magnet placement time), and Group 5: normal control group with untreated rats (n = 5). The fourth passage unlabeled or NP-labeled MSCs was dyed with DiD before administration. Each rat was injected once with 1 × 10^6 MSCs (unlabeled or NP-labeled) or PBS via the tail vein. Infused MSCs were visualized by live animal imaging (Caliper Life Sciences, USA) at 7 days post-injection. The rats were euthanized on day 7.

Table 1 Primer Sequences and Product Sizes

Symbol	Primer Sequences	Product Sizes (bp)
β-Actin	F-GCGGCAGTGGCCATCTCTT R-CTGGCCGGGACCTGACAGA	151
IL6	F-AGGAGTGGCTAAGGACCAAGACC R-TGCCGAGTAGACCTCATAGTGACC	85
IL4	F-CAAGGAACACCACGGAGAACGAG R-CTTCAAGCACGGAGGTACATCACG	92
IL10	F-AAAGCAAGGCAGTGGAGCAG R-AGTAGATGCCGGGTGGTTCA	151
Cox2	F-AGACAGATCAGAAGCGAGGACCTG R-ATACACCTCTCCACCGATGACCTG	155
TNF-α	F-GCCACGAGCAGGAATGAGAAGAG R-GCGATGTGGAACTGGCAGAGG	103
VEGF	F-GTCACCACCACACCACCATC R-GGCGAATCCAGTTCCACGAG	164
TGF-β	F-GGCACCATCCATGACATGAACCG R-GCCGTACACAGCAGTTCTTCTCTG	148

Histopathological Analysis

The dorsal skin was removed from the euthanized rats, washed with PBS, and fixed with 4% formaldehyde for at least 1 day. The skin samples were dehydrated in graded ethanol, cleared with xylene, infiltrated with paraffin wax, and embedded in paraffin. The embedded sample blocks were cut into 5-μm sections and stained with hematoxylin and eosin (H&E) for histological analysis. The sections were then washed in H_2O and tissue iron deposits were detected using the Prussian blue iron stain kit (Solarbio). Signal was enhanced with Fast 3,30–diaminobenzidine (DAB; Sigma, St Louis, MO, USA) for 2 min. The samples were then examined using an optical microscope (X51; Olympus Corporation).

Immunofluorescence Analysis

CD31 and α-SMA were detected by immunofluorescence staining to study MSC-induced angiogenesis during wound healing. Briefly, skin tissue excised from the wound sites was fixed in 4% paraformaldehyde,

dehydrated in 30% sucrose solution, embedded in OCT, and cut into 4-μm-thick sections perpendicular to the wound surface. The sections were blocked in 1% BSA for 30 min at 23–25°C, incubated with rabbit anti-CD31 (1:100; Abcam, Cambridge, UK), and mouse anti-α-SMA (1:50; Abcam) antibodies overnight at 4°C, and then stained with secondary Alexa-Fluor 594-conjugated goat anti-rabbit and Alexa-Fluor 488-conjugated goat anti-mouse secondary antibodies (Abcam, 1:200) and counter-stained with DAPI. Images were acquired using an Olympus IX81 microscope (Tokyo, Japan). The mature vessels were detected as CD31 and α-SMA double-positive vascular structures.

Statistical Analysis

All statistical analyses were performed using Statistical Package for the Social Sciences (SPSS) software (v 22.0; Chicago, IL, USA) using the nonparametric Mann–Whitney *U*-test. Data are presented as mean ± standard deviation (SD, n = 3). The results with $P<0.05$ were considered statistically significant.

Results

Characterization, Cellular Uptake, and Cytotoxicity of Fe_3O_4 NPs

The morphology of the synthesized Fe_3O_4 NPs was analyzed by TEM. Figure 2A shows a TEM image with the size distribution of magnetite NPs, demonstrating that the particles were spherical with a uniform size distribution. The NPs agglomerated due to their magnetic properties. Figure 2B shows the average Fe_3O_4 NP diameter was <60 nm. Following incubation with MSCs, the synthesized Fe_3O_4 NPs were internalized into the MSCs and localized in the cytoplasm (Figure 2C). There were no morphological differences between labeled and unlabeled MSCs (Figure 2D). NP-labeled MSCs showed typical blue deposits, which were present in nearly all Fe_3O_4 NP (50 μg/mL)-labeled MSCs. According to the ICP results (Figure 2E), 50 μg/mL NPs demonstrated the highest cellular uptake efficiency.

Next, we evaluated the cytotoxicity of Fe_3O_4 NPs at various concentrations on MSCs after labeling, and the data presented in Figure 2F show that the uptake of 50 μg/mL Fe_3O_4 NPs did not affect MSC activity. There was a decrease in the viability of cells treated with Fe_3O_4 at concentrations of > 50 μg/mL. Thus, MSCs labeled with 50 μg/mL Fe_3O_4 NPs were used in the subsequent studies.

Effect of Fe_3O_4 NPs on MSC Differentiation, CD Marker Profiles, and Proliferation in vitro

Labeling MSCs with Fe_3O_4 NPs did not affect CD marker expression. All cells expressed CD44, CD73, CD105 and CD90, and lacked CD34 and CD45 on their surface (Figure 3A). After treatment with adipogenic differentiation medium, NP-labeled MSCs were stained positive for lipid accumulation at a level similar to that of unlabeled MSCs. In addition, there was no difference in calcium deposition levels following osteogenic differentiation between the NP-labeled and unlabeled MSCs (Figure 3B). These results indicated that the differentiation potential of MSCs labeled with Fe_3O_4 NPs was similar to that of unlabeled cells. These results confirm that Fe_3O_4 NPs do not affect typical MSC characteristics.

We compared the proliferation of MSCs labeled with and without Fe_3O_4 NPs using the CCK-8 assay, which clearly revealed that the proliferation ability of MSCs labeled with 50 μg/mL Fe_3O_4 NPs was similar to that of unlabeled cells (Figure 3C). Additionally, the colony-forming assay revealed that Fe_3O_4 NP-labeled MSCs plated at a low density formed colonies (Figure 3D and E). Therefore, Fe_3O_4 NPs are a biocompatible nanomaterial for clinical applications.

Enhancement of Anti-Inflammatory Cytokine and Chemokine Secretion Profiles by NP-Labeled MSCs in vitro

To determine whether labeling MSCs with Fe_3O_4 NPs affected their secretory capability, we measured cytokine secretion by unlabeled and labeled MSCs. The C-X-C motif chemokine ligand 2 (CXCL2), granulocyte macrophage-colony-stimulating factor (GM-CSF), L-selectin, intracellular cell adhesion molecule (ICAM)-1, tissue inhibitor of metalloproteinase (TIMP)-1, and interleukin (IL)-4 levels were significantly increased in MSCs labeled with Fe_3O_4 NPs compared with those in unlabeled MSCs. There were no differences in the CXCL3 and IL-13 secretion profiles between NP-labeled and unlabeled MSCs (Figure 4).

Magnetic Targeted of MSC Migration to Burn Injury Sites and Their Therapeutic Effects in the Rat Model

We assessed MSC homing in response to severe burns in vivo by transplanting Fe_3O_4 NP-labeled or unlabeled

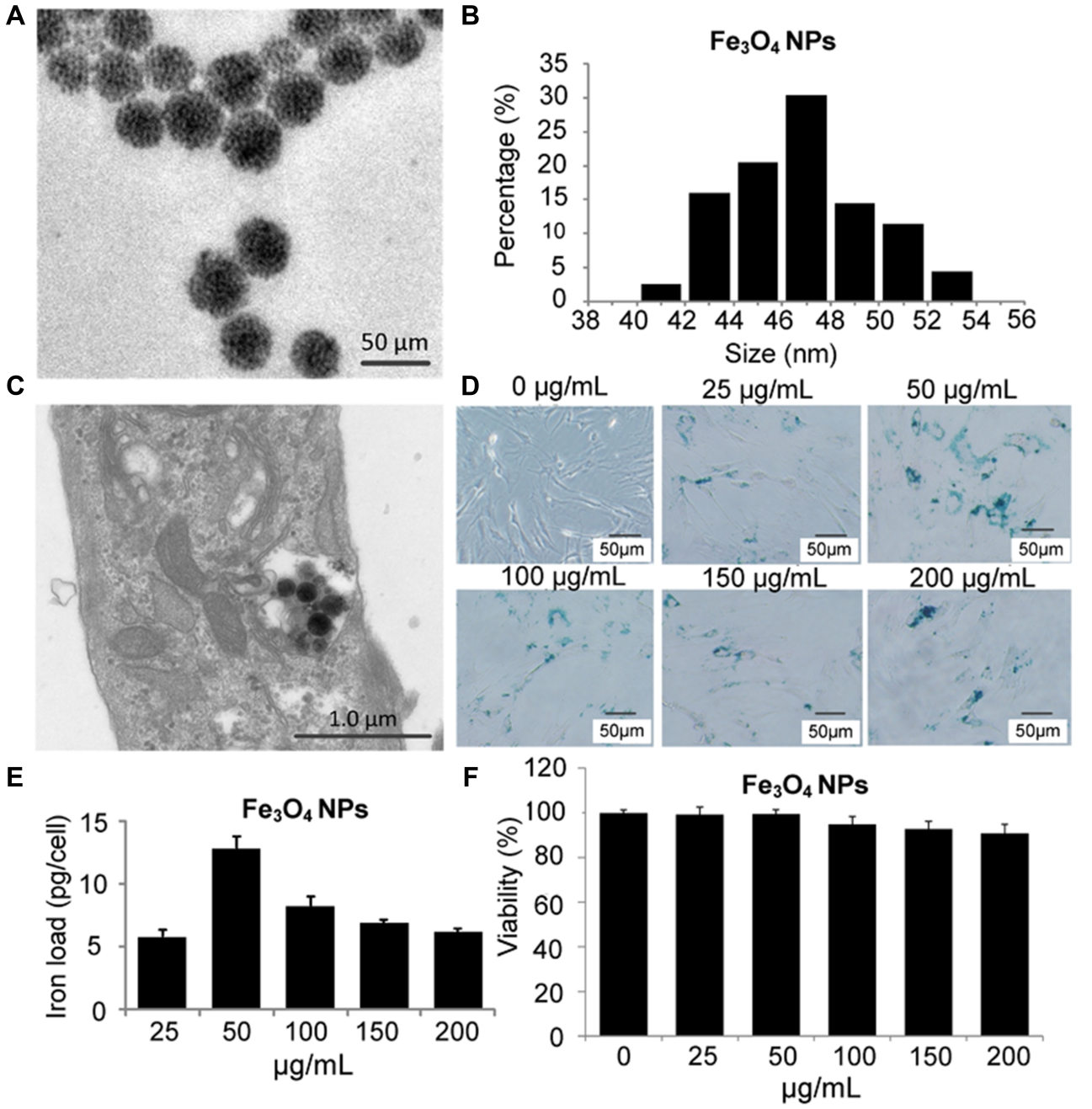

Figure 2 Fe_3O_4 NP synthesis and internalization by MSCs. (**A**) TEM image of Fe_3O_4 NPs (scale bar = 50 nm); (**B**) Size distribution of Fe_3O_4 NPs; MSCs were incubated with Fe_3O_4 NPs in FBS-free culture medium for 2 h. The cells and NPs were then co-cultured in fresh medium containing 10% FBS for 14 h. (**C**) TEM image of 50 μg/mL Fe_3O_4 NPs internalized into an MSC. Scale bar = 1.0 μm. MSCs were labeled with different NP concentrations for 16 h to define the optimum labeling efficiency. (**D**) Then, MSCs were stained with Prussian blue iron stain. Scale bar = 50 μm. (**E**) Iron concentration was determined by ICP-OES. (**F**) NP-induced cell toxicity was evaluated in MSCs labeled with NP at different concentrations for 24 h.

MSCs into rats with severe burns. The rats were then subjected to live imaging at 7 days after MSC transplantation. Unlabeled and NP-labeled MSCs were dyed with DiD before transplantation. Numerous MSCs were present in the cutaneous area of the burn wound site on days 7. Additionally, fluorescent signals in the burn wounds in rats treated with magnetically targeted MSCs were stronger than those in the other group rats on days 7 (Figure 5A). Prussian blue staining for iron with DAB enhancement showed minimal iron deposition in the burn wound sites in the Fe_3O_4 NP-labeled MSC group, while more iron deposition in the magnetically targeted MSC group (Figure 5B). These results suggest that EMF promotes homing of NP-labeled MSCs to burn injury sites in vivo.

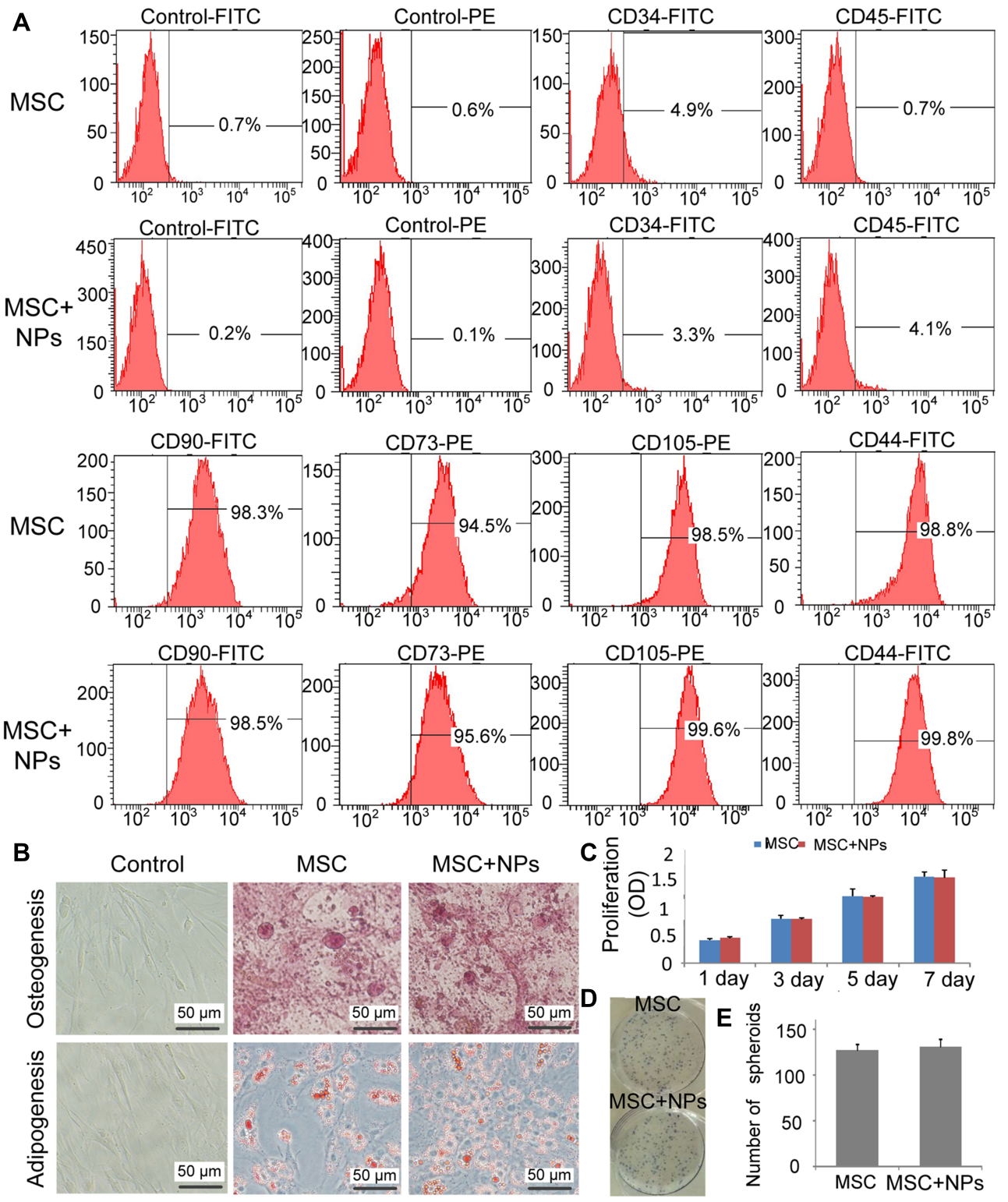

Figure 3 MSC characteristics and proliferation were not affected by Fe_3O_4 NPs. MSCs were incubated with Fe_3O_4 NPs in FBS-free culture medium for 2 h. The cells and NPs were then co-cultured in fresh medium containing 10% FBS for 14 h. (**A**) Cell marker analysis of MSC-labeled NPs showed that strong CD44, CD73, CD105, and CD90 expression, and absent CD45 and CD34 expression. (**B**) Differentiation of MSC-labeled NPs. MSCs differentiated into osteoblasts and adipocytes. (**C**) Proliferation of 50μg/mL NP-labeled MSCs was assessed after 7 days using CCK8. (**D**) Colonies of 50 μg/mL NP-labeled MSCs were stained with Giemsa stain. (**E**) The number of colonies formed was counted.

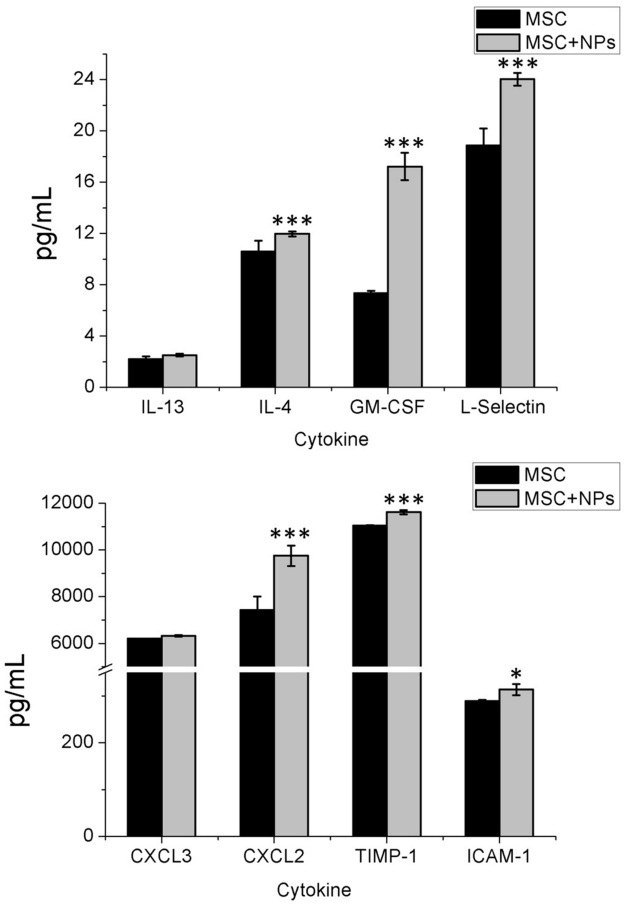

Figure 4 Cytokine release from MSCs labeled with Fe_3O_4 NPs. MSCs were incubated with Fe_3O_4 NPs in FBS-free culture medium for 2 h. The cells and NPs were then co-cultured in fresh medium containing 10% FBS for 14 h. The MSC-alone control cultures were collected at 24 h. Standard cell culture medium was used as the control. Cytokine concentrations were measured using the Luminex assay. Bars represent the SD. *p <0.05, and ***p <0.001, vs the MSC-alone group.

H&E staining of the skin burn sections showed that inflammatory cells were the primary cells infiltrating the severe burn wounds. The total number of lymphocytes in the burns of rats transplanted with MSCs, Fe_3O_4 NP-labeled MSCs, and magnetically targeted MSCs was considerably lower than that in the PBS-treated group (Figure 5C). The vascularization of newly formed tissues is an essential step in the wound healing process. In the present study, we identified vessels at wound sites by co-staining against CD31 and alpha-smooth muscle actin (α-SMA) (Figure 5D). The number of vessels increased during the healing process in all MSC-treated groups, with the magnetically targeted MSC group displaying the greatest vessel density of vessels at day 7 and the MSC group or Fe_3O_4 NP-labeled MSC-treated group having a higher vessel density of vessels than the control group.

Changes in Anti-Inflammatory Cytokine Profiles Following Treatment with Magnetically Targeted MSCs in vivo

Moreover, we evaluated cytokine levels in the serum of MSCs, Fe_3O_4 NP-labeled MSCs, and magnetically targeted MSC groups at 1, 4, and 7 days after transplantation. The IL-1α, IL-2, IL-6, and interferon (INF)-γ levels in the burn transplanted with MSCs, Fe_3O_4 NP-labeled MSCs, and magnetically targeted MSCs were lower than those in the PBS group (Figure 6). However, the level of anti-inflammatory cytokines, such as IL-10, in these groups was higher than that in the PBS group. Moreover, the VEGF level in the three MSC-transplanted groups was higher than that in the PBS group. In the magnetically targeted MSC-transplanted groups, the VEGF level was higher and IL-6 level was lower than those in the other groups. In addition, 7 days post transplantation, the IL-1α and IL-2 levels were lower in the magnetically targeted MSC group than in the other MSC groups.

Concomitant with MSC retention at burn sites, reduced pro-inflammatory gene expression, including tumor necrosis factor-α (TNF-α), *IL-6*, and cyclooxygenase 2 (*COX2*), was observed in the qRT-PCR analysis of the skin samples at 7 days (Figure 7). Additionally, a statistically significant increase in anti-inflammatory gene expression (*TGF-β, IL-4*, and *IL-10*) was observed in tissues injected with NP-labeled and unlabeled MSCs compared with those in the PBS group. *VEGF* was also upregulated in tissues injected with NP-labeled and unlabeled MSCs, with higher levels in tissues treated with magnetically targeted MSCs than in tissues treated with MSCs alone or NP-labeled MSCs.

Safety of Fe_3O_4 NPs in vivo

To evaluate the safety profile of Fe_3O_4 NPs on major rat organs in vivo, the heart, liver, spleen, lung and kidney were investigated. The data presented in Figure 8 show no obvious difference in inflammatory, apoptotic, or necrotic cells in rat tissues, indicating that Fe_3O_4 NPs did not cause obvious toxicity in vivo. Therefore, Fe_3O_4 NPs are excellent nanomaterials that can be used to study interactions between NPs and the body milieu because of their aqueous solubility.

Discussion

Effective MSC migration and homing following transplantation pose a major hurdle in the development of

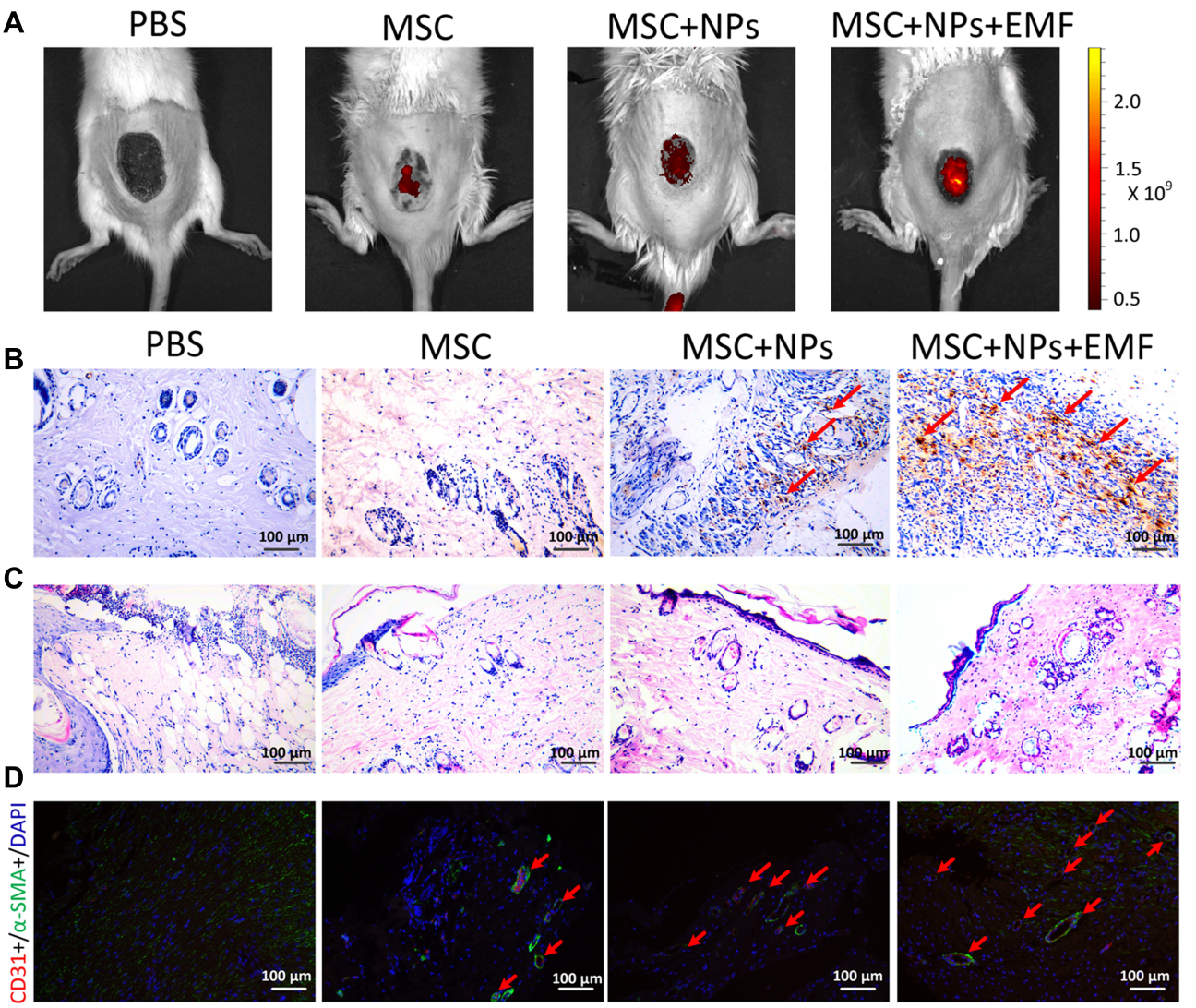

Figure 5 MSC migration to the burn injury lesions and their therapeutic effects in the rat model. (**A**) The live imaging of MSCs, labeled MSCs, and magnetically targeted MSCs in rats with burn injuries. (**B**) DAB-enhanced Prussian blue staining of skin sections at 7 days revealed that Fe_3O_4 NPs remained in the skin tissues. The red arrow indicates yellowish brown iron deposits. Scale bar = 100 μm. (**C**) Histological features of skin sections from the burned area stained with H&E at 7 days after burn induction. Scale bar = 100 μm. (**D**) Immunofluorescence staining for CD31 and α-SMA in wounds after treatment with PBS, MSCs, MSCs labeled Fe_3O_4 NPs or magnetically targeted MSCs 7 days post-wounding. The red arrow indicates vessels. Scale bar = 100 μm.

regenerative therapies. Previous studies labeled MSCs with NPs to investigate the fate of NPs following injection or to guide them to specific target areas via EMF application.[39,42] Herein, we demonstrated that NPs were effectively incorporated into MSCs without influencing MSC proliferation or viability in vitro. The application of magnetic targeting improved the in vivo homing efficiency of NP-labeled MSCs to the burn region in a rat model. Further experiments demonstrated that magnetically targeted MSCs improved cellular anti-inflammatory capacity compared with MSC treatment alone. This study provides new insights into strategies for enhancing MSC migration to wound sites, and this may contribute to the development of novel methods for treating and improving wound healing. In this study, we used commercially available NPs for cell labeling. The average size of the NPs ranged from 40 to 60 nm, which is similar to the finding of a previous study.[43] The in vitro and in vivo data confirmed that MSCs effectively internalized the NPs in the absence of any transfection agent without significantly altering MSC properties. Previous studies indicated that Fe_3O_4 NP labeling increased MSC viability, proliferation, and differentiation potential.[44,45] However, other studies reported that Fe_3O_4 NPs reduced the viability and colony-forming ability of cells.[46,47] Recent findings on the effect of NPs on cell behavior are controversial due to differences in NP

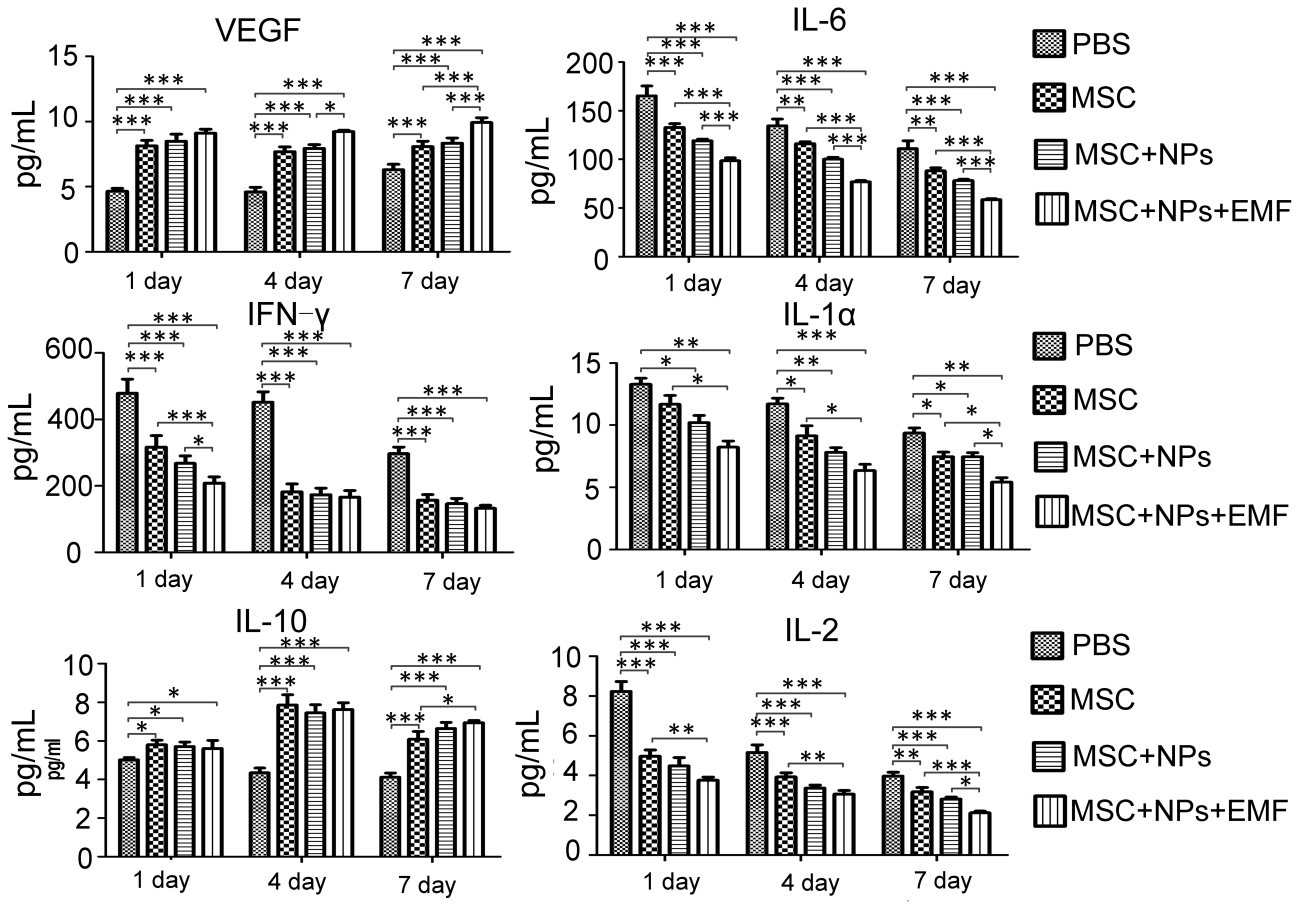

Figure 6 Cytokine level analysis in the rat model. Kinetics of cytokine levels in serum of burned rats treated with PBS, MSCs, MSCs labeled Fe_3O_4 NPs or magnetic targeting MSCs. (n = 3). Bar represent the SD. *p < 0.05, **p < 0.01, and ***p<0.001, vs the PBS group.

size, shape, surface modifications, and incubation concentration and time among studies. However, we did not observe severe adverse reactions in vivo following NP administration, which may have been due to the small size of the NPs. In addition, NPs at 50 μg/mL concentration exhibited the highest cellular uptake efficiency because higher concentrations of NPs reduce the Brownian motion, thereby precluding the cellular uptake of NP aggregates.[46] Additionally, NP tended to aggregate at higher concentrations in the culture medium and adhere to the plate.[48]

Our Luminex results revealed that the incorporation of NPs into MSCs enhances their ability to secrete anti-inflammatory cytokines and growth factors, which are vital factors for enhancing the therapeutic effect of these cells. Previous findings showed that iron oxide NPs increased ICAM-1, E-selectin, IL-6, and IL-8 production in human umbilical vein endothelial cells or human aortic endothelial cells,[49,50] whereas *CCL5* and *MMP9* were differentially upregulated in RAW264.7 cells.[51] Moreover, CXCL1, CXCL2, CXCL3, and CCL3 were differentially upregulated in iron oxide NP-loaded lung epithelial cells.[52] Iron oxide NPs also promoted the expression of genes associated with the wound healing process, including *TGFβ1, MMP2, MMP9, WNT4*, and *CTNNB1*, resulting in improved wound healing.[53] Moreover, in vitro Fe_3O_4 NP-loaded endothelial progenitor cells enhanced the migration and secretion of growth factors (VEGF and FGF), and this was associated with a moderate increase in reactive oxygen species production.[54] Hence, iron oxide NP uptake by certain cell types enhances the expression of anti-inflammatory cytokines and growth factors.

The wound healing process may be disturbed by necrosis, infection, and excess levels of inflammatory factors. If a wound is in a continuous inflammatory state, it will initiate a cascade state, resulting in a permanent nonhealing state.[55] In the present study, MSCs migrated into wound sites, and localized to the wound base and edge. Magnetic targeting increased the recruitment of

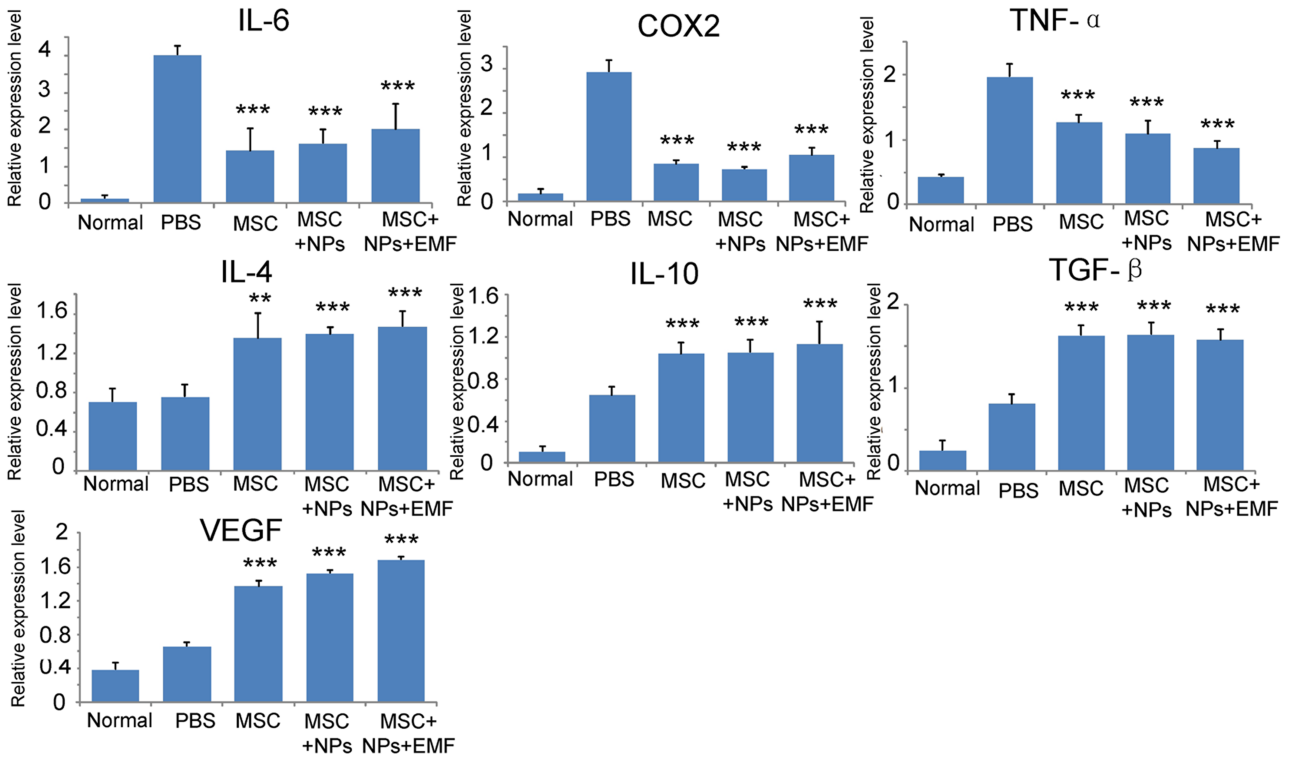

Figure 7 qRT-PCR analysis of *IL-6*, *TNF-α*, and *COX2* (pro-inflammatory); *IL-4*, *TGF-β*, and *IL-10* (anti-inflammatory); and *VEGF* genes on tissue explants at 7 days following the injection of magnetically targeted MSCs, MSCs labeled with Fe_3O_4 NPs, and unlabeled MSCs (n = 3). Bars represent the SD. **p < 0.01 and ***p < 0.001, vs the PBS group.

intravenously injected MSCs and significantly promoted anti-inflammatory effects. Our results showed that the production of the pro-inflammatory cytokines INF-γ, IL-2, IL-6, and IL-1α in the burn was significantly lower in the transplanted MSCs, NP-labeled MSCs, and magnetically targeted MSC groups than in the PBS-treated group. Furthermore, NP-labeled MSC accumulation at the injury site clearly increased the production of the anti-inflammatory cytokine IL-10, which plays a major role in the MSC anti-inflammatory cytokine profile. In a previous study, cutaneous wounds transplanted with human umbilical cord MSCs demonstrated a substantially lower number of inflammatory cells and pro-inflammatory cytokines than the PBS-treated group.[22] Magnetically targeted MSCs presented an improved inflammation-inhibiting effect at the wound site.

The process of new blood vessel formation in wounds is initiated by VEGF, which activates the endothelial cells of existing vessels.[21] In skin wounds, increasing VEGF secretion facilitates recovery and healing. The magnetically targeted MSC group appeared to exhibit higher VEGF expression than the other groups. MSC recruitment and accumulation at burn sites increased the restorative effect, and this is consistent with previous study findings.[56] The decreased expression of pro-inflammatory markers and increased expression of anti-inflammatory agents suggest that MSCs exhibit anti-inflammatory activity. Several studies have revealed that MSC-secreted paracrine nutrition factors, such as VEGF, promoted the neovascularization of injured tissues.[57] Additionally, we found that magnetic targeting enhanced the cutaneous wound healing effects of MSCs through significantly increasing the number of closed tubular structures in vitro and increasing the number of blood vessels in vivo. These results indicated that magnetically targeted MSCs could improve the blood supply in wound beds, and the number of blood vessels increasing as MSCs accumulated in the wound. Overall, these results suggest that magnetic targeting promotes the therapeutic effects of MSCs in laser-induced skin injuries.

In this study, Fe_3O_4 NPs were effectively incorporated into MSCs without altering their stem cell properties. Magnetically targeted MSCs were used in a rat laser wound model. After implantation at the injured skin site, magnetic targeting enhanced the recruitment of NP-labeled MSCs and contributed to the improvement in the anti-inflammatory ability compared with MSC treatment alone. This study

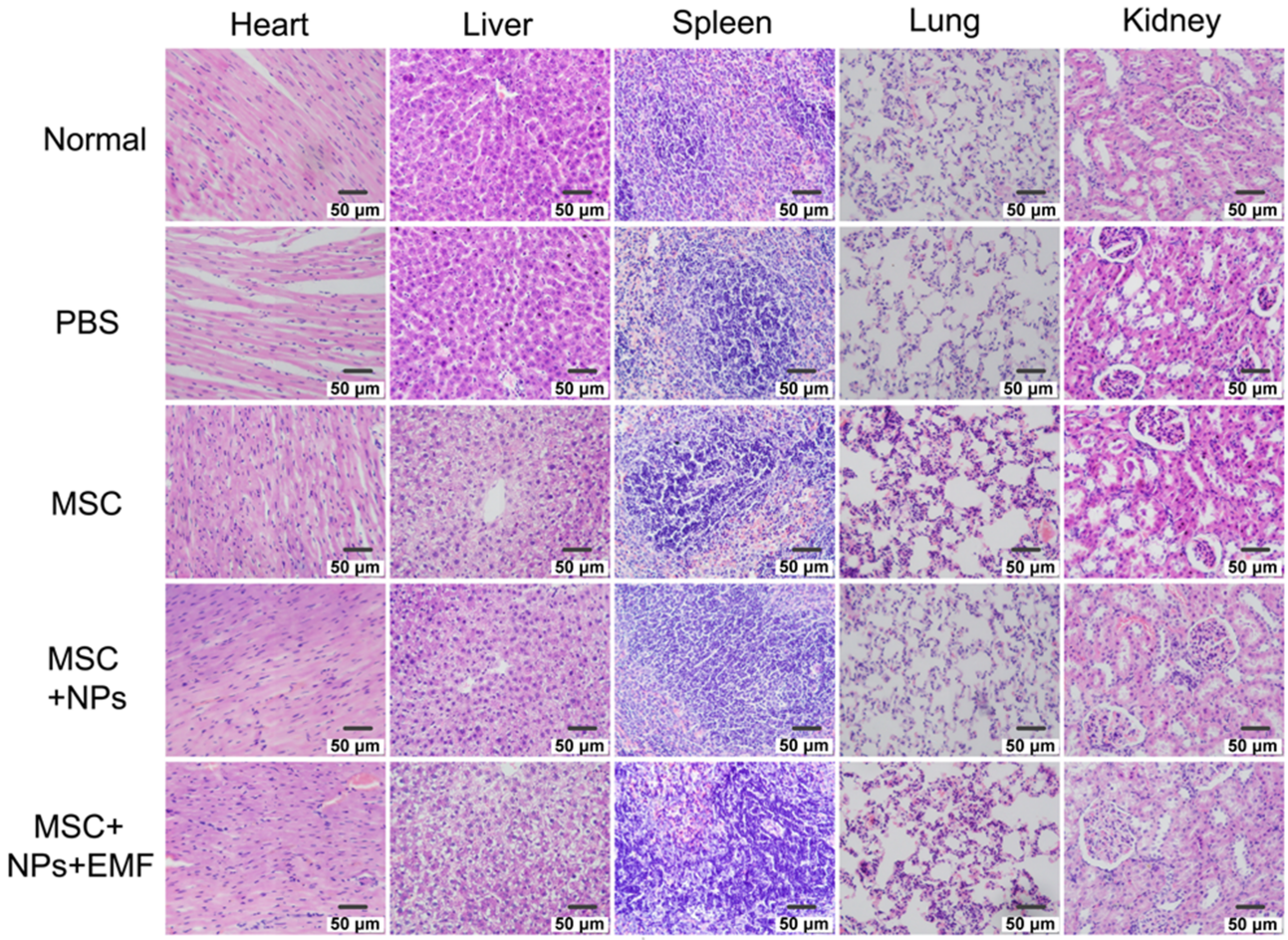

Figure 8 H&E staining of the heart, liver, spleen, lung, and kidney at 7 days after tail-vein injection of PBS, MSCs, NP-labeled MSCs, or magnetically targeted MSCs. Scale bar = 50 μm.

provides new insights into a strategy to boost MSC migration to wound sites, which may contribute to the development of novel methods for treating and enhancing wound healing.

Data Sharing Statement

The datasets used to support the findings of this study are included within the article.

Funding

This work was supported by the Science and Technology Project of Jilin Provincial Education Department (Grant Nos. 20200201310JC, 20190901007JC, 20190304030YY, and 20190908002TC), the Capital Construction Funds Planned Projects in the Provincial Budget of 2019 (Grant No. 2019C016), the Changchun Science and Technology Development Plan Project (Grant No. 18YJ011), the Health Service Capacity Improvement Project in Jilin Province (Grant No. 2017F014), and the Health Special Project of Jilin Provincial Finance Department (Grant Nos. sczsy201716 and 2018scz034).

Disclosure

The authors declare no conflicts of interest in this work.

References

1. Xu J, Zgheib C, Hodges MM, Caskey RC, Hu J, Liechty KW. Mesenchymal stem cells correct impaired diabetic wound healing by decreasing ECM proteolysis. *Physiol Genomics*. 2017;49(10):541. doi:10.1152/physiolgenomics.00090.2016
2. Alexeev V, Uitto J, Igoucheva O. Gene expression signatures of mouse bone marrow-derived mesenchymal stem cells in the cutaneous environment and therapeutic implications for blistering skin disorder. *Cytotherapy*. 2011;13(1):30–45. doi:10.3109/14653249.2010.518609
3. Ochiai H, Kishi K, Kubota Y, et al. Transplanted mesenchymal stem cells are effective for skin regeneration in acute cutaneous wounds of pigs. *Regen Ther*. 2017;7:8–16. doi:10.1016/j.reth.2017.06.003
4. Chu J, Shi P, Deng X, et al. Dynamic multiphoton imaging of acellular dermal matrix scaffolds seeded with mesenchymal stem cells in diabetic wound healing. *J Biophoton*. 2018;11(7):e201700336. doi:10.1002/jbio.201700336

5. Dave SD, Patel CN, Vanikar AV, Trivedi HL. In vitro differentiation of neural cells from human adipose tissue derived stromal cells. *Neurol India*. 2018;66(3):716–721. doi:10.4103/0028-3886.232326
6. Carmelo JG, Fernandes-Platzgummer A, Cabral JMS, Silva CLD. Scalable Ex Vivo Expansion of Human Mesenchymal Stem/Stromal Cells in Microcarrier-Based Stirred Culture Systems. *Methods Mol Biol*. 2014;1283:147–159. doi:10.1007/7651_2014_100
7. Zhang H, Li ZL, Yang F, et al. Radial shockwave treatment promotes human mesenchymal stem cell self-renewal and enhances cartilage healing. *Stem Cell Res Ther*. 2018;9:54. doi:10.1186/s13287-018-0805-5
8. Sivanathan KN, Gronthos S, Rojas-Canales D, Thierry B, Coates PT. Interferon-gamma modification of mesenchymal stem cells: implications of autologous and allogeneic mesenchymal stem cell therapy in allotransplantation. *Stem Cell Rev*. 2014;10:351–375. doi:10.1007/s12015-014-9495-2
9. Kang I, Lee BC, Lee JY, et al. Interferon-gamma-mediated Secretion of Tryptophanyl-tRNA Synthetases Has a Role in Protection of Human Umbilical Cord Blood-derived Mesenchymal Stem Cells Against Experimental Colitis. *BMB reports*. 2019;52(5):318–323. doi:10.5483/BMBRep. 2019.52.5.134
10. Roth M, Spaniol K, Kordes C, et al. The influence of oxygen on the proliferative capacity and differentiation potential of lacrimal gland–derived mesenchymal stem cells. *Invest Ophthalmol Vis Sci*. 2015;56:4741–4752. doi:10.1167/iovs.14-15475
11. Wright EJ, Hodson NW, Sherratt MJ, et al. Combined MSC and GLP-1 therapy modulates collagen remodeling and apoptosis following myocardial infarction. *Stem Cells Int*. 2016;2016:7357096. doi:10.1155/2016/7357096
12. Nitzsche F, Muller C, Lukomska B, Jolkkonen J, Deten A, Boltze J. Concise review: MSC adhesion cascade-insights into homing and transendothelial migration. *Stem Cells*. 2017;35(6):1446–1460. doi:10.1002/stem.2614
13. Yin Y, Hao H, Cheng Y, et al. The homing of human umbilical cord-derived mesenchymal stem cells and the subsequent modulation of macrophage polarization in type 2 diabetic mice. *Int Immunopharmacol*. 2018;60:235–245. doi:10.1016/j.intimp.2018.04.051
14. Collette NM, Yee CS, Hum NR, et al. Sostdc1 deficiency accelerates fracture healing by promoting the expansion of periosteal mesenchymal stem cells. *Bone*. 2016;88:20–30. doi:10.1016/j.bone.2016.04.005
15. Chen J, Wei J, Huang Y, et al. Danhong injection enhances the therapeutic efficacy of mesenchymal stem cells in myocardial infarction by promoting angiogenesis. *Front Physiol*. 2018;9:991. doi:10.3389/fphys.2018.00991
16. Luo L, Tang J, Nishi K, et al. Fabrication of synthetic mesenchymal stem cells for the treatment of acute myocardial infarction in mice. *Circ Res*. 2017;120:1768–1775. doi:10.1161/CIRCRESAHA.116.310374
17. Madrigal M, Rao KS, Riordan NH. A review of therapeutic effects of mesenchymal stem cell secretions and induction of secretory modification by different culture methods. *J Transl Med*. 2014;12(1):260. doi:10.1186/s12967-014-0260-8
18. Hop MJ, Polinder S, Middelkoop E, van BM. Costs of Burn Care: A Systematic Review. *Value Health*. 2014;17(7):A606. doi:10.1016/j.jval.2014.08.2111
19. Ennis WJ, Sui A, Bartholomew A. Stem Cells and Healing: impact on Inflammation. *Adv Wound Care*. 2013;2(7):369–378. doi:10.1089/wound.2013.0449
20. Rajabian MH, Ghorabi GH, Geramizadeh B, Sameni S, Ayatollahi M. Evaluation of bone marrow derived mesenchymal stem cells for full-thickness wound healing in comparison to tissue engineered chitosan scaffold in rabbit. *Tissue Cell*. 2017;49(1):112–121. doi:10.1016/j.tice.2016.11.002
21. Lee DE, Ayoub N, Agrawal DK. Mesenchymal stem cells and cutaneous wound healing: novel methods to increase cell delivery and therapeutic efficacy. *Stem Cell Res Ther*. 2016;7(1):37. doi:10.1186/s13287-016-0303-6
22. Liu L, Yu Y, Hou Y, et al. Human umbilical cord mesenchymal stem cells transplantation promotes cutaneous wound healing of severe burned rats. *PLoS One*. 2014;9(2):e88348. doi:10.1371/journal.pone.0088348
23. Perez-Diaz MA, Silva-Bermudez P, Jimenez-Lopez B, et al. Silver-pig skin nanocomposites and mesenchymal stem cells: suitable anti-biofilm cellular dressings for wound healing. *J Nanobiotechnology*. 2018;16(1):2. doi:10.1186/s12951-017-0331-0
24. Xu J, Wu W, Zhang L, et al. The role of MicroRNA-146a in the pathogenesis of the diabetic wound-healing impairment: correction with mesenchymal stem cell treatment. *Diabetes*. 2012;61(11):2906–2912. doi:10.2337/db12-0145
25. Iyer SS, Rojas M. Anti-inflammatory effects of mesenchymal stem cells: novel concept for future therapies. *Expert Opin Biol Ther*. 2008;8(5):569–581. doi:10.1517/14712598.8.5.569
26. Levy O, Mortensen LJ, Boquet G, et al. A small-molecule screen for enhanced homing of systemically infused cells. *Cell Rep*. 2015;10:1261–1268. doi:10.1016/j.celrep.2015.01.057
27. Dykstra B, Lee J, Mortensen LJ, et al. Glycoengineering of E-Selectin Ligands by Intracellular versus Extracellular Fucosylation Differentially Affects Osteotropism of Human Mesenchymal Stem Cells. *Stem Cells*. 2016;34:2501–2511. doi:10.1002/stem.2435
28. Brenner S, Whiting-Theobald N, Kawai T, et al. CXCR4-transgene expression significantly improves marrow engraftment of cultured hematopoietic stem cells. *Stem Cells*. 2004;22:1128–1133. doi:10.1634/stemcells.2003-0196
29. Huang J, Zhang Z, Guo J, et al. Genetic modification of mesenchymal stem cells overexpressing CCR1 increases cell viability, migration, engraftment, and capillary density in the injured myocardium. *Circ Res*. 2010;106:1753–1762. doi:10.1161/CIRCRESAHA.109.196030
30. Kalimuthu S, Oh JM, Gangadaran P, et al. In vivo tracking of chemokine receptor CXCR4-engineered mesenchymal stem cell migration by optical molecular imaging. *Stem Cells Int*. 2017;2017:8085637. doi:10.1155/2017/8085637
31. Furumoto T, Ozawa N, Inami Y, et al. Mallotus philippinensis bark extracts promote preferential migration of mesenchymal stem cells and improve wound healing in mice. *Phytomedicine*. 2014;21:247–253. doi:10.1016/j.phymed.2013.09.003
32. Jordan A, Scholz R, Maier-Hauff K, et al. Presentation of a new magnetic field therapy system for the treatment of human solid tumors with magnetic fluid hyperthermia. *J Magn Magn Mater*. 2001;225(1):118–126.
33. Jun YW, Lee JH, Cheon J. *Angew Chem Int Ed Engl*.
34. Hou CH, Hou SM, Hsueh YS, Lin J, Wu HC, Lin FH. The in vivo performance of biomagnetic hydroxyapatite nanoparticles in cancer hyperthermia therapy. *Biomaterials*. 2009;30:3956–3960. doi:10.1016/j.biomaterials.2009.04.020
35. Na HB, Song IC, Hyeon T. Inorganic nanoparticles for MRI contrast agents. *Adv Mater*. 2010;21:2133–2148. doi:10.1002/adma.200802366
36. Cores J, Caranasos TG, Cheng K. Magnetically targeted stem cell delivery for regenerative medicine. *J Funct Biomater*. 2015;6(3):526–546. doi:10.3390/jfb6030526
37. Silva LH, Cruz FF, Morales MM, Weiss DJ, Rocco PR. Magnetic targeting as a strategy to enhance therapeutic effects of mesenchymal stromal cells. *Stem Cell Res Ther*. 2017;8:58. doi:10.1186/s13287-017-0523-4
38. Chen Z, Yin JJ, Zhou YT, et al. Dual enzyme-like activities of iron oxide nanoparticles and their implication for diminishing cytotoxicity. *ACS Nano*. 2012;6:4001–4012. doi:10.1021/nn300291r
39. Shen WB, Plachez C, Tsymbalyuk O, et al. Cell-based therapy in TBI: magnetic retention of neural stem cells in vivo. *Cell Transplant*. 2016;25:1085–1099. doi:10.3727/096368915X689550
40. Qi Y, Feng G, Huang Z, Weiqi Y. The application of super paramagnetic iron oxide-labeled mesenchymal stem cells in cell-based therapy. *Mol Biol Rep*. 2013;40:2733–2740. doi:10.1007/s11033-012-2364-7

41. Nakano M, Nagaishi K, Konari N, et al. Bone marrow-derived mesenchymal stem cells improve diabetes-induced cognitive impairment by exosome transfer into damaged neurons and astrocytes. *Sci Rep*. 2016;6(1):24805. doi:10.1038/srep24805
42. Zhu LL, Zhang Z, Jiang HS, Chen H, Chen Y, Dai YT. Superparamagnetic iron oxide nanoparticle targeting of adipose tissue-derived stem cells in diabetes-associated erectile dysfunction. *Asian J Androl*. 2017;19:425–432. doi:10.4103/1008-682X.179532
43. Ge R, Li X, Lin M, et al. Fe3O4@ polydopamine composite theranostic superparticles employing preassembled Fe3O4 nanoparticles as the core. *ACS Appl Mater Interfaces*. 2016;8(35):22942–22952. doi:10.1021/acsami.6b07997
44. Huang DM, Hsiao JK, Chen YC, et al. The promotion of human mesenchymal stem cell proliferation by superparamagnetic iron oxide nanoparticles. *Biomaterials*. 2009;30:3645–3651. doi:10.1016/j.biomaterials.2009.03.032
45. Wang Q, Chen B, Cao M, et al. Response of MAPK pathway to iron oxide nanoparticles in vitro treatment promotes osteogenic differentiation of hBMSCs. *Biomaterials*. 2016;86:11–20. doi:10.1016/j.biomaterials.2016.02.004
46. Pernal S, Wu VM, Uskokovic V. Hydroxyapatite as a vehicle for the selective effect of superparamagnetic iron oxide nanoparticles against human glioblastoma cells. *ACS Appl Mater Interfaces*. 2017;9(45):39283–39302. doi:10.1021/acsami.7b15116
47. Schafer R, Kehlbach R, Muller M, et al. Labeling of human mesenchymal stromal cells with superparamagnetic iron oxide leads to a decrease in migration capacity and colony formation ability. *Cytotherapy*. 2009;11(1):68–78. doi:10.1080/14653240802666043
48. Li X, Wei Z, Lv H, et al. Iron oxide nanoparticles promote the migration of mesenchymal stem cells to injury sites. *Int J Nanomedicine*. 2019;14:573–589. doi:10.2147/IJN.S184920
49. Wagner M, Klein CL, van Kooten TG, Kirkpatrick CJ. Mechanisms of cell activation by heavy metal ions. *J Biomed Mater Res*. 1998;42(3):443–452. doi:10.1002/(SICI)1097-4636(19981205)42:3<443::AID-JBM14>3.0.CO;2-H
50. Zhu MT, Wang B, Wang Y, et al. Endothelial dysfunction and inflammation induced by iron oxide nanoparticle exposure: risk factors for early atherosclerosis. *Toxicol Lett*. 2011;203:162–171. doi:10.1016/j.toxlet.2011.03.021
51. Liu Y, Chen Z, Gu N, Wang J. Effects of DMSA-coated Fe3O4 magnetic nanoparticles on global gene expression of mouse macrophage RAW264.7 cells. *Toxicol Lett*. 2011;205(2):130–139. doi:10.1016/j.toxlet.2011.05.1031
52. Teeguarden JG, Mikheev VB, Minard KR, et al. Comparative iron oxide nanoparticle cellular dosimetry and response in mice by the inhalation and liquid cell culture exposure routes. *Part Fibre Toxicol*. 2014;11(1):46. doi:10.1186/s12989-014-0046-4
53. Moniri M, Boroumand Moghaddam A, Azizi S, et al. Molecular study of wound healing after using biosynthesized BNC/Fe<sub>3O4 nanocomposites assisted with a bioinformatics approach. *Int J Nanomedicine*. 2018;13:2955–2971. doi:10.2147/IJN.S159637
54. Carenza E, Barcelo V, Morancho A, et al. In vitro angiogenic performance and in vivo brain targeting of magnetized endothelial progenitor cells for neurorepair therapies. *Nanomedicine*. 2014;10(1):225–234. doi:10.1016/j.nano.2013.06.005
55. Choi H, Lee RH, Bazhanov N, Oh JY, Prockop DJ. Anti-inflammatory protein TSG-6 secreted by activated MSCs attenuates zymosan-induced mouse peritonitis by decreasing TLR2/NF-κB signaling in resident macrophages. *Blood*. 2011;118(2):330–338. doi:10.1182/blood-2010-12-327353
56. Lu J, Shen X, Sun X, et al. Increased recruitment of endogenous stem cells and chondrogenic differentiation by a composite scaffold containing bone marrow homing peptide for cartilage regeneration. *Theranostics*. 2018;8:5039–5058. doi:10.7150/thno.26981. eCollection 2018
57. Wang Y, Wang M, Abarbanell AM, et al. MEK mediates the novel cross talk between TNFR2 and TGF-EGFR in enhancing vascular endothelial growth factor (VEGF) secretion from human mesenchymal stem cells. *Surgery*. 2009;146(2):198–205. doi:10.1016/j.surg.2009.04.013

International Journal of Nanomedicine Dovepress

Publish your work in this journal

The International Journal of Nanomedicine is an international, peer-reviewed journal focusing on the application of nanotechnology in diagnostics, therapeutics, and drug delivery systems throughout the biomedical field. This journal is indexed on PubMed Central, MedLine, CAS, SciSearch®, Current Contents®/Clinical Medicine, Journal Citation Reports/Science Edition, EMBase, Scopus and the Elsevier Bibliographic databases. The manuscript management system is completely online and includes a very quick and fair peer-review system, which is all easy to use. Visit http://www.dovepress.com/testimonials.php to read real quotes from published authors.

Submit your manuscript here: https://www.dovepress.com/international-journal-of-nanomedicine-journal